Acta Crystallographica Section B
Structural Science
ISSN 0108-7681

On the crystal chemistry of olivine-type germanate compounds, $Ca_{1+x}M_{1-x}GeO_4$ (M^{2+} = Ca, Mg, Co, Mn)

Günther J. Redhammer,[a]* Georg Roth,[b] Georg Amthauer[a] and Werner Lottermoser[a]

[a]Department of Materials Engineering and Physics, Division of Mineralogy, University of Salzburg, Hellbrunnerstrasse 34, A-5020 Salzburg, Austria, and [b]Institute of Crystallography, RWTH Aachen, Jägerstrasse 17/19, D-52056 Aachen, Germany

Correspondence e-mail: guenther.redhammer@aon.at

Received 16 June 2007
Accepted 15 April 2008

Germanate compounds, $CaMGeO_4$ with M^{2+} = Ca, Mg, Co and Mn, were synthesized as single crystals by slow cooling from the melt or by flux growth techniques. All the compositions investigated exhibit *Pnma* symmetry at 298 K and adopt the olivine structure. The *M*2 site is exclusively occupied by Ca^{2+}, while on *M*1 both Ca^{2+} and M^{2+} cations are found. The amount of Ca^{2+} on *M*1 increases with the size of the *M*1 cation, with the smallest amount in the Mg compound (0.1 atoms per formula unit) and the largest in the Mn compound (0.20 atoms per formula unit), while in Ca_2GeO_4, also with olivine structure, both sites are completely filled with Ca^{2+}. When compared with those of Ca silicate olivine, the lattice parameters *a* and *c* are distinctly larger in the analogous germanate compounds, while *b* has essentially the same values, regardless of the tetrahedral cation, meaning that *b* is independent of the tetrahedral cation. Structural variations on the octahedrally coordinated *M*1 site are largely determined by the size of the *M*1 cation, the average *M*1—O bond lengths being identical in Ca silicate and Ca germanate olivine. Increasing the size of the *M*1 cation induces an increasing polyhedral distortion, expressed by the parameters bond-length distortion, octahedral angle variance and octahedral quadratic elongation. However, the Ca germanate olivine compounds generally have more regular octahedra than the analogous silicates. The octahedrally coordinated *M*2 site does not exhibit large variations in structural parameters as a consequence of the constant chemical composition; the same is valid for the tetrahedral site.

1. Introduction

The olivine structure type is frequently found, both in natural and in synthetic compounds. Olivine itself, $(Fe,Mg)_2SiO_4$, is the most abundant material of the Earth's mantle and a huge amount of information is available for this mineral group (see *e.g.* Brown, 1980; Deer *et al.*, 1997). The olivine structure is also realized in many other A_2BX_4 compounds, among them synthetic $LiInSiO_4$ (Redhammer & Roth, 2003), triphylite ($LiFePO_4$; Losey *et al.*, 2004; Streltsov *et al.*, 1993; a material that has been intensively studied recently because of its potential application as an electrode material in Li batteries), alexandrite (Al_2BeO_4:Cr; examined within our group: Weber *et al.*, 2007), and sinhalite ($MgAlBO_4$; Hayward *et al.*, 1994).

The olivine structure contains two distinct octahedrally coordinated metal sites *M* (with *M*1 on special position 4*a*, site symmetry $\bar{1}$, and *M*2 on special position 4*c*, site symmetry *m*) and one isolated tetrahedrally coordinated polyhedron (*T*, also in special position 4*c*, *Pnma* setting). The dominant feature of the olivine structure is a stretched infinite chain of edge-sharing *M*1 octahedra parallel to the *b* axis. At the same

Table 1
Chemical composition of selected $CaM^{2+}GeO_4$ olivine compounds of this study, as determined by electron microprobe analysis.

	CaCo_a1	CaCo_a2	Ca2Co_2	CaMg_a1	Ca2Mg_1	CaMn_a2	Ca2Mn_1	CaZn_b
Oxide weight percent (wt%)								
CaO	26.39 (13)	26.01 (15)	28.91 (11)	32.08 (14)	29.84 (12)	29.57 (11)	32.26 (14)	51.46 (12)
MgO	–	–	–	16.70 (6)	18.27 (6)	–	–	–
CoO	28.59 (9)	29.01 (8)	25.97 (8)	–	–	–	–	–
MnO	–	–	–	–	–	25.25 (7)	21.18 (7)	–
GeO_2	44.79 (6)	44.50 (8)	45.31 (8)	51.07 (11)	51.52 (9)	45.49 (7)	46.88 (9)	48.32 (7)
Sum	99.78	99.53	100.18	99.85	99.63	100.31	99.82	99.69
Stoichiometric coefficients								
Ca^{2+}	1.11	1.09	1.19	1.16	1.08	1.20	1.31	1.99
Mg^{2+}	–	–	–	0.84	0.92	–	–	–
Co^{2+}	0.90	0.91	0.80	–	–	–	–	–
Mn^{2+}	–	–	–	–	–	0.81	0.68	–
Ge^{4+}	1.01	1.00	1.00	0.99	1.00	0.99	1.01	1.00

Compound IDs define the nominal composition of the starting material: CaCo_ = $CaCoGeO_4$, Ca2Co_ = $Ca_2CoGe_2O_7$, CaMg_ = $CaMgGeO_4$, Ca2Mg_ = $Ca_2MgGe_2O_7$, CaMn_ = $CaMnGeO_4$, Ca2Mn_ = $Ca_2MnGe_2O_7$ and CaZn_ = $CaZnGeO_4$, numbers behind '_' are internal crystal numbers.

z height, the $M2$ octahedra are attached to this chain on opposite sides of a central $M1$ octahedron by common edges; thus the $M1$ and $M2$ sites together are described as an infinite zigzag chain parallel to **b** (*e.g.* Brown, 1980; Lager & Meagher, 1978). Zigzag chains in layers above and below are separated by an $a/2$ displacement along the ⟨102⟩ direction. The $M1$ octahedron shares six of its O—O edges with adjacent polyhedra – two with $M1$, two with $M2$ and two with the neighbouring tetrahedron – while the $M2$ polyhedron shares two edges with $M1$ and one with the tetrahedron, all of these edges belonging to the same triangular face of the $M2$ octahedron. The tetrahedra are isolated from each other, having the apex pointing up and down, and crosslink the M chains of different layers along the **c** direction. Fig. 1(*a*) displays part of the olivine structure, containing the asymmetric unit and some symmetry-related atoms including the symmetry codes, while Fig. 1(*b*) displays the complete unit cell.

In silicate olivine at ambient conditions (Brown, 1980) it is accepted that large divalent cations (Ca^{2+}, Mn^{2+}) tend to order onto the $M2$ site, while small cations preferentially occupy the $M1$ site. It was also found that Co^{2+} shows a strong preference for the $M1$ site, for example in Co^{2+} olivine ($Co_{1.1}Mg_{0.9}SiO_4$; Ghose & Wan, 1974). Recent work mainly focused on *in-situ* experiments to study cation ordering at high temperatures (Rinaldi *et al.*, 2000, 2005; Redfern *et al.*, 1997, 2000; Henderson *et al.*, 1996; Artioli *et al.*, 1995). These studies revealed a crossover in ordering behaviour at high temperatures; for example, Fe^{2+} prefers the $M2$ site above ∼900 K in $(Mg,Fe)SiO_4$ olivine (Artioli *et al.*, 1995; Redfern *et al.*, 2000). Similarly Mn^{2+} shows a preference for the $M2$ site at low temperatures but becomes increasingly disordered between $M1$ and $M2$ (Redfern *et al.*, 1997), while Co^{2+} shows a distinct preference for $M1$, even at high temperature (Rinaldi *et al.*, 2005).

While silicate olivine is studied frequently, investigations of analogous germanate compounds are rare. Single-crystal structure determinations with the relevant data are only available for $CaMgGeO_4$ (van Duijn *et al.*, 1995). Eulenberger *et al.* (1962) reported the synthesis of Ca_2GeO_4 and found the olivine structure for it, but no additional data are given. Mn_2GeO_4, Ca_2GeO_4 and $CaMgGeO_4$ were investigated up to pressures of ∼30 GPa using X-ray diffraction and X-ray absorption spectroscopy (Petit *et al.*, 1996) and by high-pressure Raman spectroscopy (Reynard *et al.*, 1997). Structural phase transitions have been observed above 6 and 12 GPa for Ca_2GeO_4 and $CaMgGeO_4$, respectively (Petit *et al.*, 1996); the nature of the structural changes, however, remains uncertain. It was noted, though, that analogous germanate compounds are more suitable, for example, for high-pressure experiments, as phase transitions appear to take place at distinctly lower pressures than in the silicate compounds (Petit *et al.*, 1996).

In this present contribution the atomic arrangement of a series of synthetic Ca germanate olivines is determined from

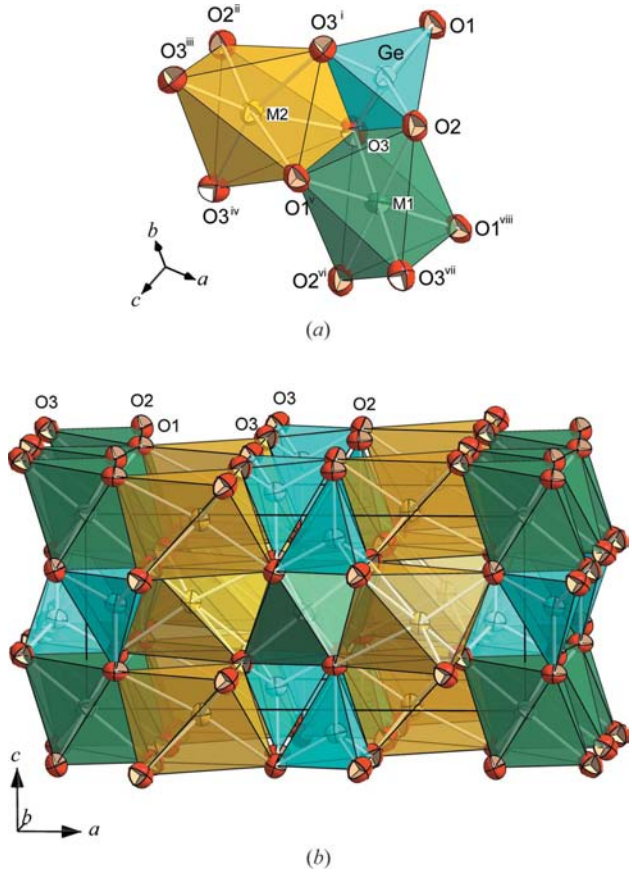

Figure 1
(*a*) A view of the asymmetric unit and some symmetry-related atoms of Ca_2GeO_4, showing 95% probability displacement ellipsoids and the atomic nomenclature scheme [symmetry codes: (i) $x, \frac{1}{2}-y, z$; (ii) $-\frac{1}{2}+x, \frac{1}{2}-y, \frac{1}{2}-z$; (iii) $\frac{1}{2}-x, \frac{1}{2}+y, \frac{1}{2}+z$; (iv) $\frac{1}{2}-x, -y, \frac{1}{2}+z$; (v) $x, y, 1+z$; (vi) $1-x, -\frac{1}{2}+y, 1-z$; (vii) $1-x, -y, 1-z$; (viii) $1-x, -\frac{1}{2}+y, -z$]. (*b*) A full polyhedral representation of the olivine structure.

Table 2
Data collection parameters and results of structure refinement for selected $CaM^{2+}GeO_4$ olivine compounds of this study.

	CaMg_a1	CaCo_a1	CaMn_a2	Ca2Mn_1	CaZn_b
Crystal data					
Chemical formula	$Ca_{1.16}GeMg_{0.83}O_4$	$Ca_{1.11}Co_{0.89}GeO_4$	$Ca_{1.17}GeMn_{0.83}O_4$	$Ca_{1.31}GeMn_{0.69}O_4$	GeO_4.1.99(Ca)
M_r	203.52	233.55	229.16	227.02	216.37
Cell setting, space group	Orthorhombic, *Pnma*	Orthorhombic, *Pnma*	Orthorhombic, *Pnma*	Orthorhombic, *Pnma*	Orthorhombic, *Pnma*
Temperature (K)	295 (2)	295 (2)	295 (2)	295 (2)	295 (2)
a, b, c (Å)	11.2916 (7), 6.4405 (4), 5.0251 (3)	11.2873 (7), 6.4369 (4), 5.0245 (3)	11.3256 (7), 6.5643 (4), 5.1098 (3)	11.3391 (7), 6.6035 (4), 5.1326 (3)	11.3919 (7), 6.7800 (4), 5.2424 (3)
α, β, γ (°)	90, 90, 90	90, 90, 90	90, 90, 90	90, 90, 90	90, 90, 90
V (Å^3)	365.44 (4)	365.06 (4)	379.89 (4)	384.32 (4)	404.91 (4)
Z	4	4	4	4	4
D_x (Mg m^{-3})	3.7	4.249	4.007	3.924	3.55
Radiation type	Mo $K\alpha$	Mo $K\alpha$	Mo $K\alpha$	Mo $K\alpha$	Mo $K\alpha$
μ (mm^{-1})	10.01	13.71	12.14	11.74	9.96
Crystal form, colour	Cuboid, colourless	Cuboid, pink	Cuboid, brown	Cuboid, brown	Cuboid, colourless
Crystal size (mm)	0.07 × 0.05 × 0.04	0.13 × 0.12 × 0.09	0.18 × 0.15 × 0.14	0.14 × 0.12 × 0.11	0.13 × 0.12 × 0.09
Data collection					
Diffractometer	Bruker SMART APEX	Bruker SMART APEX	Bruker SMART APEX	Bruker SMART APEX	Bruker SMART APEX
Data collection method	ω scans	ω scans	ω scans	ω scans	ω scans
Absorption correction	Numerical	Numerical	Numerical	Numerical	Numerical
T_{min}	0.55	0.19	0.23	0.21	0.29
T_{max}	0.67	0.30	0.34	0.27	0.42
No. of measured, independent and observed reflections	4411, 542, 536	4315, 531, 528	4624, 555, 548	4316, 517, 510	4870, 595, 588
Criterion for observed reflections	$I > 2\sigma(I)$	$I > 2\sigma(I)$	$I > 2\sigma(I)$	$I > 2\sigma(I)$	$I > 2\sigma(I)$
R_{int}	0.036	0.040	0.058	0.054	0.039
θ_{max} (°)	29.7	29.3	29.5	28.4	29.4
No. and frequency of standard reflections					
Intensity decay (%)					
Refinement					
Refinement on	F^2	F^2	F^2	F^2	F^2
$R[F^2 > 2\sigma(F^2)]$, $wR(F^2)$, S	0.022, 0.051, 1.22	0.021, 0.049, 1.20	0.021, 0.050, 1.22	0.020, 0.045, 1.24	0.018, 0.044, 1.24
No. of reflections	542	531	555	517	595
No. of parameters	43	43	45	44	41
H-atom treatment	No H atoms present	No H atoms present	No H atoms present	No H atoms present	No H atoms present
Weighting scheme	$w = 1/[\sigma^2(F_o^2) + (0.0229P)^2 + 0.4844P]$, where $P = (F_o^2 + 2F_c^2)/3$	$w = 1/[\sigma^2(F_o^2) + (0.0183P)^2 + 1.0355P]$, where $P = (F_o^2 + 2F_c^2)/3$	$w = 1/[\sigma^2(F_o^2) + (0.0218P)^2 + 0.2627P]$, where $P = (F_o^2 + 2F_c^2)/3$	$w = 1/[\sigma^2(F_o^2) + (0.0157P)^2 + 0.6189P]$, where $P = (F_o^2 + 2F_c^2)/3$	$w = 1/[\sigma^2(F_o^2) + (0.019P)^2 + 0.4001P]$ where $P = (F_o^2 + 2F_c^2)/3$
$(\Delta/\sigma)_{max}$	<0.0001	<0.0001	<0.0001	<0.0001	<0.0001
$\Delta\rho_{max}$, $\Delta\rho_{min}$ (e Å^{-3})	0.77, −0.61	0.66, −0.58	0.8, −0.65	0.78, −0.96	0.69, −0.45
Extinction method	None	*SHELXL*	*SHELXL*	None	*SHELXL*
Extinction coefficient	–	0.0090 (10)	0.0288 (18)	–	0.0145 (14)

Computer programs used: *SMART-Plus*, *SAINT-Plus* (Bruker, 2001), *SHELXS*97, *SHELXL*97 (Sheldrick, 2008), *DIAMOND* Version 3.0 (Pennington, 1999), *WinGX* Version 1.70.01 (Farrugia, 1999).

single-crystal X-ray diffraction data at ambient conditions, and crystal–chemical comparison is made with the analogous silicate olivine. Structural investigations at non-ambient conditions are in progress and will be reported elsewhere.

2. Experimental

2.1. Material synthesis

Single crystals of germanate olivines were obtained either by slow cooling from the melt (self-flux) or by flux-growth techniques using $CaCl_2$ as the high-temperature solvent. In a first set of experiments, the olivine-type compounds were synthesized by chance during attempts to synthesize $Ca_2M^{2+}Ge_2O_7$-type compounds (M^{2+} = Mg, Ni, Co and Mn) similar to $Ca_2ZnGe_2O_7$ (Redhammer & Roth, 2006). Finely ground, homogeneous mixtures of $CaCO_3$, GeO_2 and M-oxides (MgO, NiO, Co_2O_3 and MnO) with the stoichiometry of $Ca_2M_2Ge_2O_7$ were filled into small platinum tubes (20 mm in length, 3 mm inner diameter, welded tight on one side, the other side open), put into a chamber furnace and heated from room temperature to 1773 K within 12 h. The temperature was stabilized at 1773 K for 24 h and then slowly decreased to 1273 K at a rate of 3 K h^{-1}. The products of the

Table 3
Selected structural and polyhedral distortion parameters for the Ge olivine compounds given in Table 2.

Bond lengths are given in Å, BLD in %, volume in Å^3, and OAV and TAV in °; TQE and OQE are dimensionless. Polyhedral volumes were calculated using the program *XTALDRAW* (Downs, 2005).

*M*1 site	O1	O2	O3	⟨*M*1—O⟩	BLD†	*V*	OAV‡	OQE§
CaCo_a1	2.180 (2)	2.147 (2)	2.185 (2)	2.171	0.73	13.20	79.27	1.0217
CaMg_a1	2.191 (2)	2.140 (2)	2.179 (2)	2.170	0.93	13.19	81.00	1.0222
CaMn_a2	2.262 (2)	2.217 (2)	2.276 (2)	2.252	1.03	14.58	104.50	1.0289
Ca2Mn_1	2.277 (2)	2.234 (2)	2.295 (2)	2.268	1.02	14.86	112.55	1.0313
CaZn_b	2.351 (2)	2.330 (2)	2.409 (2)	2.363	1.29	16.53	150.48	1.0425

*M*2 site	O1	O2	O3	O3	⟨Ca—O⟩	BLD	*V*	OAV	OQE
CaCo_a1	2.439 (2)	2.313 (2)	2.434 (2)	2.296	2.369	2.83	16.84	124.36	1.0355
CaMg_a1	2.455 (2)	2.317 (2)	2.433 (2)	2.298	2.372	2.87	16.90	125.76	1.0358
CaMn_a2	2.436 (2)	2.305 (2)	2.440 (2)	2.309	2.373	2.75	16.98	118.51	1.0337
Ca2Mn_1	2.444 (2)	2.308 (2)	2.443 (2)	2.323	2.381	2.64	17.12	120.31	1.0341
CaZn_b	2.446 (2)	2.296 (2)	2.462 (2)	2.362	2.398	2.43	17.43	130.68	1.0371

T site	O1	O2	O3	⟨Ge—O⟩	BLD	*V*	TAV†	TQE‡
CaCo_a1	1.746 (2)	1.775 (2)	1.760 (2)	1.760	0.43	2.73	73.72	1.0168
CaMg_a1	1.740 (2)	1.776 (2)	1.756 (2)	1.757	0.54	2.71	77.86	1.0177
CaMn_a2	1.735 (2)	1.776 (2)	1.761 (2)	1.758	0.66	2.73	60.20	1.0135
Ca2Mn_1	1.735 (2)	1.773 (2)	1.761 (2)	1.757	0.64	2.73	59.34	1.0133
CaZn_b	1.745 (2)	1.780 (2)	1.763 (2)	1.763	0.51	2.77	46.67	1.0106

† BLD = $(100/n)\sum_{i=1}^{n}|(X-\mathrm{O})_i - \langle X-\mathrm{O}\rangle|/\langle X-\mathrm{O}\rangle$ %. n is the number of cation–anion bonds and X—O = cation–anion (oxygen) distance (Renner & Lehmann, 1986). ‡ OAV = $\sum_{i=1}^{12}(\Theta_i - 90^\circ)^2/11$, where Θ_i is the O—M—O bonding angle (Robinson *et al.*, 1971). § OQE = $\sum_{i=1}^{6}(l_i/l_o)^2/6$, where l_o is the centre-to-vertex distance for a regular octahedron whose volume is equal to that of the undistorted tetrahedron with bond length l_i (Robinson *et al.*, 1971). † TAV = $\sum_{i=1}^{6}(\Theta_i - 109.57^\circ)^2/5$, with Θ_i = O—T—O bonding angle (Robinson *et al.*, 1971). ‡ TQE = $\sum_{i=1}^{4}(l_i/l_t)^2/4$, where l_t is the centre-to-vertex distance for a regular tetrahedron whose volume is equal to that of the undistorted octahedron with bond length l_i (Robinson *et al.*, 1971).

syntheses were the following three pairs: olivine-type $CaMgGeO_4$ and spinel-type Mg_2GeO_4, $CaCoGeO_4$ and traces of dark-pink Co_2GeO_4 spinel, and $CaMnGeO_4$ and glass; for the experiment with M^{2+} = Ni the synthesis batch consisted of Ni_2GeO_4 as the main phase with a minor component of $Ca_5Ge_3O_{11}$ (Barbier & Levy, 1997).

In a second step, oxide mixtures in the stoichiometry of olivine-type material $CaM^{2+}GeO_4$ (M^{2+} = Mg, Zn, Ni, Co and Mn) were used for synthesis. Again, the finely ground, homogeneous starting materials were put into Pt tubes; however, the temperature treatment was slightly altered: heating to 1623 K within 24 h, stabilizing at this temperature for another 24 h and slow cooling to 1273 K at a rate of 2.8 K h^{-1}. For the second series, experimental batches consisted of olivine-type $CaMgGeO_4$, $CaCoGeO_4$ with minor traces of Co_2GeO_4 spinel and $CaMnGeO_4$ with traces of glass. The experiment with M^{2+} = Ni again yielded Ni_2GeO_4 spinel as the main phase with some $Ca_5Ge_3O_{11}$ (presumably containing traces of Ni, as concluded from its pale olive-green colour); the experiment with Zn resulted in large crystals of Zn_2GeO_4 (up to 1 mm in size) and a minor component of monoclinic $Ca_2ZnGe_2O_7$ (Redhammer & Roth, 2006).

Ca_2GeO_4 was grown using a high-temperature solution method with $CaCl_2$ as the flux. $CaCl_2$ was added to a stoichiometric mixture of $CaCO_3$ and GeO_2 in a ratio of edduct to flux of 1:2. The assemblage was put into a platinum crucible, covered with a lid and heated in a chamber furnace to 1273 K, held for 24 h at 1273 K, and cooled to 1073 K at a rate of 4 K h^{-1}. After soaking the flux with hot distilled water, large colourless crystals of Ca_2GeO_4 up to 2 mm in size were obtained. The method is similar to that described by Bykov *et al.* (2000) for the synthesis of Ca_2GeO_4:Cr^{4+} crystals. We also attempted to apply the flux-growth technique with $CaCl_2$ to the synthesis of $CaZnGeO_4$ and $CaNiGeO_4$ using the same flux-to-nutrient ratio and an identical temperature program. After soaking the flux, the synthesis batches consisted of large crystals of Ca_2GeO_4 and fine-grained Ni or Zn spinel, respectively. From this result it is concluded that it is not possible to grow $CaNiGeO_4$ or $CaZnGeO_4$ olivine-type germanates at ambient pressures.

2.2. Chemical analysis

The chemical composition of selected samples was determined by electron microprobe analysis. Crystal aggregates of the synthesis batches were embedded in epoxy resin, polished, covered with carbon and analysed with a Jeol JXA 8600 electron microprobe (acceleration voltage 15 kV, initial beam current 40 nA, beam focused to 5 µm). At least three different grains of each composition were analysed, with a minimum of ten analyses per grain. For all samples investigated, the crystals were homogeneous both within a grain and from grain to grain. The results of chemical analysis are given in Table 1.

2.3. Single-crystal X-ray diffraction

Suitable single crystals were glued onto glass capillaries with diameters of 100 µm. Intensity data sets were collected on a Bruker SMART APEX 4K CCD system (Mo $K\alpha$ radiation, crystal–detector distance = 60 mm, ω scans at four different φ positions, frame width = 0.3°). Lattice parameters determined from single-crystal X-ray diffraction data agree well with those determined from powder X-ray diffraction. Absorption correction was performed empirically *via* symmetry equivalents using the *SHAPE* software (Stoe & Cie, 1996). Structure solution (using Patterson methods) and subsequent refinement was carried out with the programs *SHELXS*97 and *SHELXL*97 (Sheldrick, 2008), as implemented in the program suite *WinGX* (Version 1.64; Farrugia, 1999). X-ray scattering factors for the relevant ions, together with anomalous dispersion coefficients, were taken from the *International Tables for Crystallography* (1992, Vol. C).

Table 4
Selected structural and polyhedral distortion parameters for silicate olivines as recalculated from literature data.

Compound	ICSD No.	Ref.	r_M (Å)	a (Å)	b (Å)	c (Å)	⟨M1—O⟩ (Å)	BLD (%)	OAV (°)	⟨M2—O⟩ (Å)	BLD (%)	OAV (°)	⟨Si—O⟩ (Å)	BLD (°)	TAV (°)
Ca silicate series															
$Ca_{1.00}Mg_{0.93}Fe_{0.07}SiO_4$	100646	lag	0.862	11.1110	6.3830	4.8250	2.129	3.43	103.94	2.369	2.91	168.13	1.638	1.65	48.52
$Ca_{0.98}Mn_{0.87}Mg_{0.10}SiO_4$	100650	lag	0.901	11.1510	6.4880	4.9130	2.209	1.47	133.52	2.366	2.56	165.01	1.635	0.41	33.13
$Ca_{1.00}Mg_{0.31}Fe_{0.69}SiO_4$	83825	fol	0.881	11.1640	6.4470	4.8750	2.182	0.91	123.69	2.369	2.88	167.77	1.639	0.49	34.68
$Ca_{1.00}Mg_{0.22}Fe_{0.78}SiO_4$	83824	fol	0.880	11.1660	6.4480	4.8770	2.179	1.22	122.02	2.368	2.91	168.82	1.639	0.51	33.96
$Ca_{1.26}Co_{0.74}SiO_4$	68351	kim	0.901	11.1500	6.4530	4.8660	2.180	1.44	121.29	2.366	2.71	167.87	1.637	0.54	32.91
$Ca_{1.00}Mg_{1.00}SiO_4$	202280	sha	0.860	11.1050	6.3810	4.8210	2.133	4.38	100.75	2.373	2.81	164.33	1.625	1.56	50.75
$Ca_{1.00}Mg_{0.88}Fe_{0.12}SiO_4$	79792	pil	0.864	11.1098	6.3894	4.8281	2.136	3.17	104.13	2.365	2.87	166.52	1.637	0.63	42.40
$Ca_{1.00}Mg_{1.00}SiO_4$	34591	onk	0.860	11.1080	6.3820	4.8220	2.131	3.51	110.36	2.370	2.68	174.24	1.626	0.59	43.30
$Ca_{1.00}Mg_{1.00}SiO_4$	68753	del	1.000	11.2250	6.7600	5.0780	2.352	1.35	209.47	2.392	1.65	180.82	1.646	0.38	27.21
M_2SiO_4 series															
Mg_2SiO_4	68755	del	0.720	10.2070	5.9800	4.7560	2.095	1.18	96.30	2.133	3.33	90.57	1.635	0.60	49.08
$Mg_{1.20}Fe_{0.77}Mn_{0.01}SiO_4$	64954	del	0.745	10.3270	6.0310	4.7860	2.124	1.67	109.79	2.152	3.75	104.37	1.636	0.59	43.10
Fe_2SiO_4	64901	del	0.780	10.4700	6.0860	4.8180	2.157	2.33	143.51	2.184	4.03	134.87	1.620	0.70	36.33
Ni_2SiO_4	64952	del	0.700	10.1230	5.9140	4.7310	2.083	0.81	93.41	2.101	2.15	77.80	1.632	0.71	51.13
$Ca_{0.02}Mg_{0.06}Fe_{1.80}Mn_{0.12}SiO_4$	64953	del	0.783	10.5080	6.1000	4.8260	2.158	1.94	71.42	2.168	9.24	67.31	1.728	5.29	35.06
Fe_2SiO_4	26375	fuj	0.780	10.4788	6.0873	4.8195	2.161	2.32	130.09	2.177	4.46	124.92	1.636	0.52	36.72
Mn_2SiO_4	26376	fuj	0.820	10.5964	6.2567	4.9023	2.206	1.33	138.78	2.227	3.52	126.98	1.639	0.61	36.14
$Mg_{0.17}Mn_{1.83}SiO_4$	100433	fra	0.797	10.5890	6.2340	4.8790	2.187	1.42	128.35	2.228	3.85	125.39	1.639	0.86	35.65
$Mg_{1.84}Fe_{0.16}$	40726	pri	0.725	10.2242	5.9908	4.7624	2.101	1.24	99.15	2.136	3.39	93.39	1.635	0.61	48.92
$Mg_{1.83}Fe_{0.17}Ni_{0.02}$	40727	pri	0.725	10.2292	5.9919	4.7619	2.102	1.27	99.02	2.136	3.40	94.03	1.635	0.64	48.61
$Mg_{1.83}Fe_{0.16}Ni_{0.01}SiO_4$	40728	pri	0.725	10.2264	5.9912	4.7625	2.101	1.26	99.05	2.136	3.33	93.47	1.635	0.63	49.73
$Mg_{1.79}Fe_{0.20}Ni_{0.01}SiO_4$	40729	pri	0.726	10.2314	5.9947	4.7365	2.102	1.25	98.03	2.137	3.44	93.73	1.636	0.70	48.47
$Mg_{1.64}Fe_{0.36}SiO_4$	40730	pri	0.731	10.2642	6.0071	4.7688	2.109	1.36	102.79	2.142	3.50	97.67	1.635	0.60	46.72
$Mg_{1.62}Fe_{0.38}SiO_4$	40731	pri	0.731	10.2659	6.0130	4.7704	2.110	1.35	102.96	2.144	3.64	98.35	1.636	0.57	45.81
$Mg_{1.21}Fe_{0.79}SiO_4$	40732	pri	0.744	10.3273	6.0307	4.7861	2.124	1.58	109.31	2.153	3.80	104.32	1.636	0.57	43.87
$Mg_{1.06}Fe_{0.90}Mn_{0.04}SiO_4$	40733	pri	0.749	10.3475	6.0423	4.7901	2.130	1.61	112.80	2.156	3.80	107.15	1.636	0.52	42.63
$Mg_{0.35}Fe_{1.55}Mn_{0.11}SiO_4$	40734	pri	0.772	10.4712	6.0933	4.8207	2.157	2.08	127.17	2.181	4.31	121.59	1.635	0.46	36.60
$Mg_{0.15}Fe_{1.74}Mn_{0.11}SiO_4$	40735	pri	0.778	10.4959	6.0960	4.8256	2.160	2.10	127.67	2.190	5.04	143.74	1.637	0.45	38.88
$Mg_{0.14}Fe_{1.74}Mn_{0.12}SiO_4$	40736	pri	0.778	10.5095	6.0980	4.8269	2.161	2.22	129.52	2.184	4.23	123.96	1.638	0.47	38.60
$Mg_{0.11}Fe_{1.74}Mn_{0.12}SiO_4$	40737	pri	0.779	10.5084	6.0996	4.8245	2.162	2.18	130.27	2.185	4.24	124.89	1.635	0.47	37.77
$Mg_{0.08}Fe_{1.74}Mn_{0.12}SiO_4$	40738	pri	0.780	10.5084	6.1028	4.8267	2.161	2.18	129.11	2.186	4.32	123.96	1.638	0.44	38.18
$Mg_{2.00}SiO_4$	20270	boe	0.720	10.1985	5.9792	4.7549	2.095	1.12	95.06	2.129	3.29	89.75	1.636	0.63	47.72
$Mg_{1.40}Ni_{0.60}SiO_4$	20271	boe	0.714	10.1993	5.9567	4.7447	2.093	0.97	91.49	2.121	3.10	85.42	1.637	0.66	46.37
$Mg_{1.28}Ni_{0.72}SiO_4$	20272	boe	0.713	10.1947	5.9508	4.7437	2.091	0.98	91.26	2.120	2.99	84.95	1.638	0.60	47.08
$Mg_{1.98}Ni_{1.02}SiO_4$	20273	boe	0.710	10.1830	5.9430	4.7389	2.090	0.90	89.93	2.105	2.40	81.77	1.638	0.63	45.99
$Mg_{0.62}Ni_{1.38}SiO_4$	20274	boe	0.706	10.1612	5.9317	4.7352	2.086	0.87	88.52	2.110	2.64	78.04	1.638	0.71	48.95
$Mg_{0.50}Ni_{1.50}SiO_4$	20275	boe	0.705	10.1565	5.9285	4.7331	2.086	0.86	88.66	2.107	2.59	77.05	1.639	0.70	48.66
Ni_2SiO_4	20276	boe	0.700	10.1209	5.9150	4.7298	2.080	0.76	87.98	2.100	2.40	72.93	1.615	1.72	52.86

References: Lag: Lager & Meagher (1978); fol: Folco & Mellini (1997); kim: Kimata & Nishida (1987); sha: Sharp *et al.* (1987); pil: Pilati *et al.* (1995); onk: Onken (1965); del: Della Giusta *et al.* (1990); fuj: Fujino *et al.* (1981); fra: Francis & Ribbe (1980); pri: Princivalle & Secco (1985); boe: Boström (1987). For definitions of parameters BLD, OAV and TAV see Table 2.

3. Results and discussion

The analysis of systematic absences and intensity statistics indicated space group *Pnma* for all samples of this study. In contrast to the literature, it was decided to use the standard setting of space group No. 62, *Pnma*, instead of the non-standard *Pbnm* setting that is commonly used for olivine. Data can easily be converted to the lattice parameters and coordinates of the *Pbnm* setting by applying the transformation matrix vector (0 0 1, 1 0 0, 0 1 0). Full-matrix least-squares refinements based on F^2 using anisotropic atomic displacement parameters converged to $R_1 < 2.5\%$ for all data sets. Independently from the electron microprobe analysis (Table 1), the chemical composition of the samples was determined from site occupation refinement. It was found that the $M2$ site is fully and exclusively occupied by Ca^{2+}, while on the $M1$ site there is a disorder of M^{2+} and Ca^{2+}. The amount of Ca^{2+} found on $M1$ is small in the compound with nominal composition $CaMgGeO_4$ (∼0.1–0.15 atoms per formula unit) but increases with increasing size of the M^{2+} cation up to ∼0.3 in nominal $CaMnGeO_4$. The tetrahedral site was assumed to be completely filled by Ge^{4+}. The total amount of Ca^{2+} and Me^{2+} found by site occupation refinement is in very close agreement with the composition found by electron microprobe analysis. The cation distribution for the synthetic samples, formed directly from the melt, is as expected, with the larger Ca^{2+} cation occupying the $M2$ site, while Mg^{2+}, Co^{2+} and Mn^{2+} are ordered on $M1$. As the samples were grown above 1273 K the additional enrichment of Ca^{2+} onto $M1$ can be seen in the light of the preference of larger cations for $M1$ at high temperatures.

Table 2 contains a summary of experimental conditions during data collection and structural refinement parameters

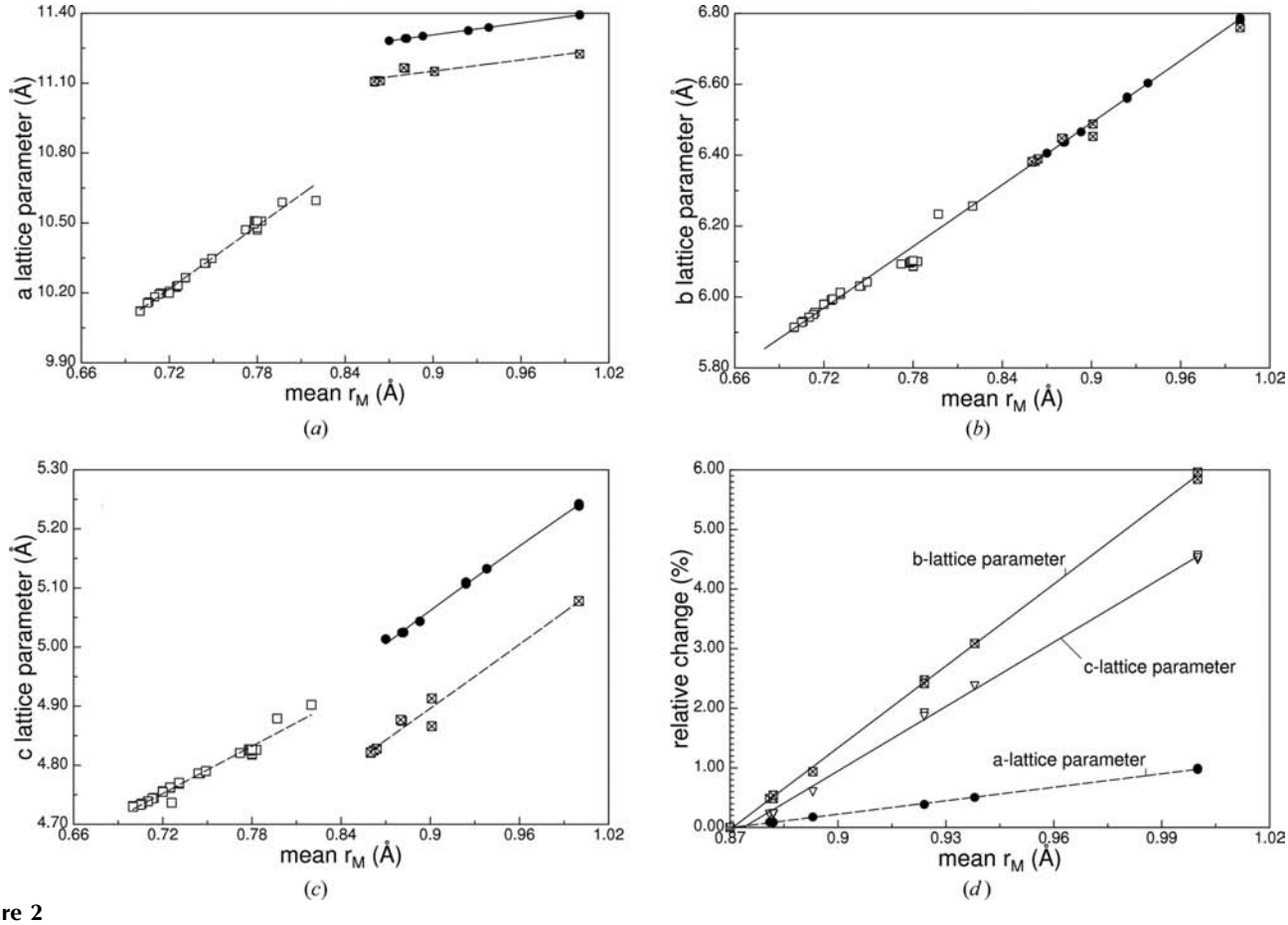

Figure 2
Lattice parameters of Ge olivines of this study in comparison with literature data [the mean radius is defined as $r_M = (\langle r_{M1}\rangle + \langle r_{M2}\rangle)/2$]; filled circles: this study; open circles: Ca silicate olivines; crossed squares: M_2SiO_4 olivines (M = Ni, Mg, Co, Fe and Mn). References to literature data are compiled in Table 4; standard deviations are smaller than the symbols if not displayed; lines fitted to the data are guides to the eye.

for five selected samples; the refined fractional atomic coordinates and equivalent isotropic and anisotropic displacement parameters have been deposited,[1] together with the complete set of single-crystal data for all the 11 samples investigated. Table 3 compiles selected bond lengths, bond angles and distortion parameters, while Table 4 contains structural parameters for some Ca silicate and M_2SiO_4 olivine compounds, recalculated from literature data using the lattice parameters and fractional atomic coordinates as given in the Inorganic Crystal Structure Database (ICSD, 2006).

3.1. Lattice parameters

The lattice parameters of the Ge olivines are largely controlled by the size of the octahedral cation. In the following, structural parameters are displayed as a function of the average octahedral cation radius $r_M = \langle r_{M1}\rangle + \langle r_{M2}\rangle)/2$, calculated from refined $M1$ and $M2$ site compositions and the ionic radii given by Shannon & Prewitt (1969). The variations of a, b and c with r_M (Fig. 2) appear to be linear and have a similar slope to the data for the Ca silicate olivines. Interestingly, the data for the b lattice parameters for Ca silicate and Ca germanate olivines plot onto each other, regardless of the fact that Ge^{4+} has a distinctly larger ionic radius than Si^{4+} (0.40 and 0.26, respectively). This result demonstrates that the b dimension is actually unaffected by substitutions on the tetrahedral site. In addition, the a axes (the long ones) are only ~1.4% longer in the germanate than in the silicate, while the c axes (the short lattice parameter) are between 8.2 and 9.7% longer in the germanate compounds, identifying this axis as the most sensitive to the replacement of Si^{4+} by Ge^{4+}.

When comparing the Ca olivines with the M_2SiO_4 olivines (M = Ni, Mg, Co, Fe and Mn) it is evident that only the b lattice parameter exhibits a common trend with r_M for all olivines and that, especially for the long axis (here a), distinct differences in slope and dimension are observable. For both a and c there is an evident discontinuity in the data between M_2SiO_4 and $CaMSiO_4$ olivines.

In the Ca germanate olivines of this study, the introduction of M^{2+} onto $M1$ causes an anisotropic expansion of the lattice (Fig. 2d), with the b lattice parameter showing the largest variation with r_M, while the a lattice parameter only expands by 1% between $CaMgGeO_4$ and Ca_2GeO_4. The largest expansion of the lattice is thus parallel to the $M1$-chain direction, while along a the Ca^{2+} sites seem to buffer the

[1] Supplementary data for this paper are available from the IUCr electronic archives (Reference: WS5059). Services for accessing these data are described at the back of the journal.

increasing size of the *M*1 cation when changing from Mg^{2+} to Ca^{2+}.

3.2. The *M*1 site

The average *M*1—O bond lengths for the olivine samples are linearly correlated with the average radius of the *M*1 cation, r_{M1} (Fig. 3*a*), and display similar values for samples with *M*2 = Ca^{2+}, regardless of the type of tetrahedral cation. Furthermore, individual *M*1—O bond lengths are similar in both the Ca germanate and the Ca silicate olivines. This behaviour shows that the substitution of the tetrahedral cation has little influence on the size requirements of the *M*1 site. Data for the M_2SiO_4 olivines are slightly off the common trend of the Ca olivines, with similar individual *M*1—O3 and shorter *M*1—O1^{v} and *M*1—O2^{vi} bond lengths (see Fig. 1 for symmetry codes). The size enhancement of the *M*1 cation in the Ca germanate olivines causes a direction-dependent increase of individual *M*1—O bond lengths (Fig. 3*b*), with the M1—O3 bond length – being aligned approximately along the ⟨102⟩ direction – increasing most distinctly (by 11.2% from the Mg to the Ca composition), while *M*1—O1^{v} increases by 7.5% in the same r_{M1} range. As a consequence, the bond-length distortion parameter (BLD; Renner & Lehmann, 1986) slightly increases with r_{M1}, although the BLD is small compared with those for the Ca silicate olivines and most of the M_2SiO_4 olivines (Table 4). Among the octahedral oxygen–oxygen edges, the largest enhancements with r_{M1} are found for the unshared edges O2$^{vi}\cdots$O3 and O1$^{viii}\cdots$O3 (with an increase of 14.9 and 11.3%, respectively), while the O2$\cdots$O3 edge, common to the *M*1 octahedron and the Ge tetrahedron, is distinctly hampered in expansion and increases by only 2.4%. The increase of the O$\cdots$O edges with r_{M1} is linear in all cases. The different increase of the octahedral edges with increasing size of the *M*1 cation directly affects the distortional state of the *M*1 polyhedron, *i.e.* the deviation from ideal octahedral geometry, expressed by the distortion parameters octahedral angle variance (OAV) and octahedral quadratic elongation (OQE), both as defined by Robinson *et al.* (1971). Within the Ca germanate series the OAV increases distinctly and is almost twice as large in Ca_2GeO_4 as in $CaMgGeO_4$.

Two reasons for this effect are (i) the decrease of the O2—*M*1—O3 angle, opposite to the common O2$\cdots$O3 edge between *M*1 and the tetrahedral site, from 77.6 (1) to 71.3(1)° (−8.2%) and (ii) the opening up of the O2—*M*1—O3^{vii} angle, opposite to the unshared O2$\cdots$O3^{vii} edge, from 102.4 (1) to 108.7 (1)° (+6.2%). Generally, in all three series, the M_2SiO_4, the Ca silicate and the Ca germanate olivines, the OAV

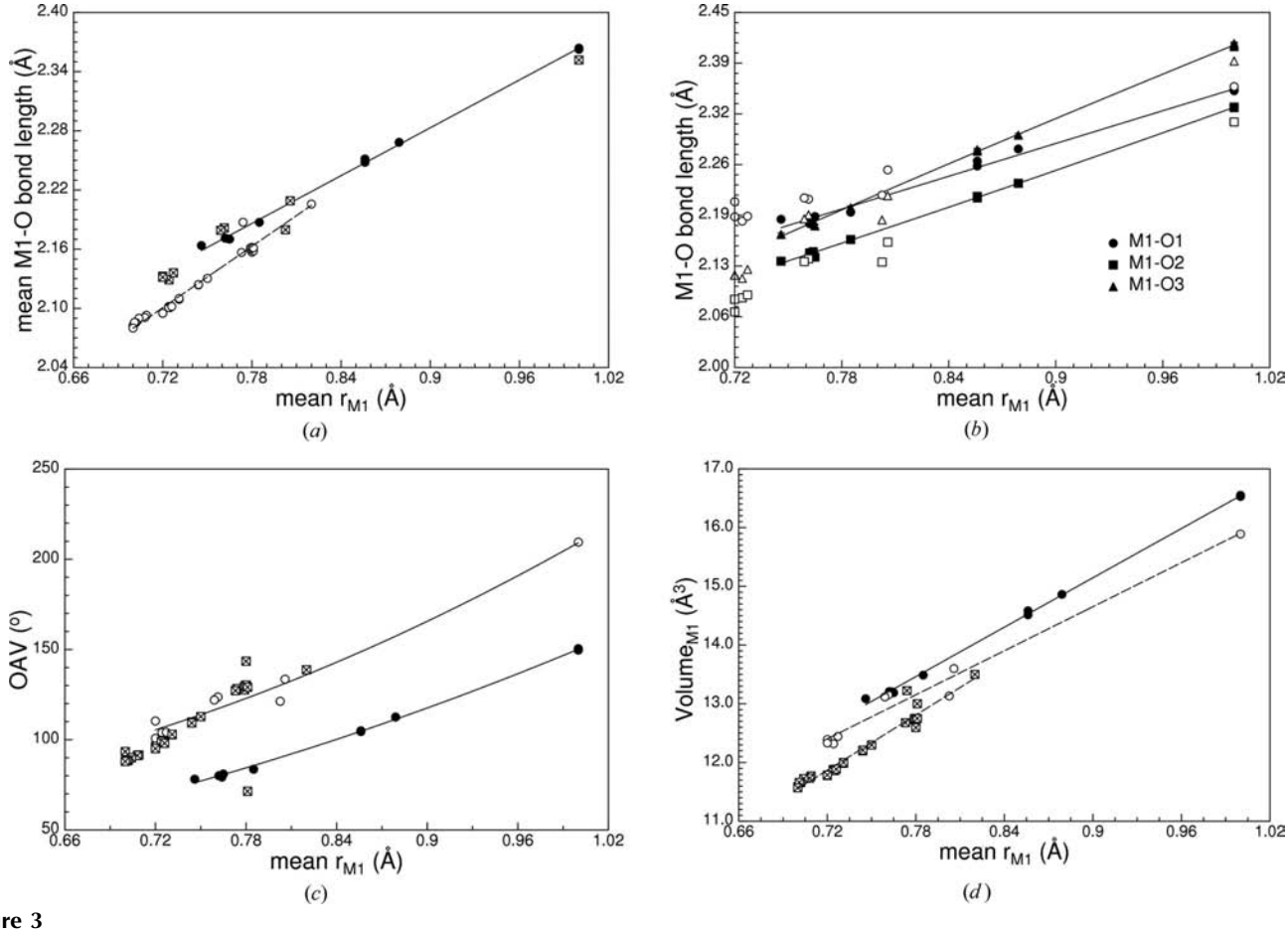

Figure 3
Variation of derived structural parameters with the average cationic radius of the *M*1 site for the Ge olivines of this study in comparison with literature data: (*a*) average *M*1—O bond length, (*b*) individual *M*1—O bond lengths, (*c*) octahedral angle variance (Robinson *et al.*, 1971) and (*d*) volume; symbols as in Fig. 2.

increases with r_{M1} (Fig. 3*c*), the *M*1 site in the germanate olivines being more regular than those in the other two series. The same observation is made for the OQE (not shown, for the sake of brevity). The volume of the *M*1 polyhedron increases linearly with r_{M1} for the Ca germanate olivines (Fig. 3*d*). It is also evident that the germanate olivines display a larger polyhedral volume than the Ca silicate olivines, and the latter have larger volumes than the M_2SiO_4 olivines (Fig. 3*d*). The volume of the *M*1 octahedron also depends on the composition of neighbouring polyhedra and increases with increasing size of the neighbouring cations (Ca^{2+} and Ge^{4+}).

3.3. The *M*2 site

For the purpose of comparison with M_2SiO_4 olivine, variations of structural parameters for the *M*2 site are displayed as a function of the average cationic radius r_M (as defined above). Within the Ca germanate series, no substitution takes place at the *M*2 site; thus, *a priori*, one would not expect any distinct alterations within the size and shape of the *M*2 polyhedron. Indeed, there are only small variations of average *M*2—O (Ca—O) bond lengths within the Ca olivine series and – similarly to the *M*1—O bond lengths – the Ca—O bond lengths are close to each other in the germanate and the silicate series, regardless of the chemical identity of the tetrahedral cation. An extrapolation of the r_M variation with average *M*2—O bond length for the M_2SiO_4 olivine samples fits the data well for pure Ca_2SiO_4 (Fig. 4*a*). Individual Ca—O bond lengths, however, do not show a uniform variation with r_M within the Ca germanate series (Fig. 4*b*); the Ca—O1^{v} bond length remains almost constant and Ca—O2^{ii} decreases by ~1%. Both bonds point in the **a** direction, which – as mentioned above – displays the smallest expansion upon *M*1-cation substitution. Conversely, the Ca—O3 and Ca—O3^{iii} bonds increase by 1.1 and 2.7%, respectively. The latter two bonds point in directions having additional components along **b** and **c** and thus are affected by the *M*1-site substitutions. In general, the variation of the individual *M*2—O bonds becomes similar with increasing r_M within the Ca germanate series, as expressed by a linear decrease of the bond-length distortion (Fig. 4*c*). Ca silicate olivines have similar (small) BLD parameters, while for the M_2SiO_4 olivine samples there is an increase of BLD with r_M for small *M*1 cations, and for larger average cationic sizes BLD decreases; the largest BLD values were calculated for Fe_2SiO_4-rich or pure Fe_2SiO_4 (fayalite) samples (Table 4). Among the oxygen–oxygen edges of the *M*2 octahedron, the O3$^{iii}\cdots$O3^{iv} edge, parallel to the *b* axis, increases by as much as 9.1% from $CaMgGeO_4$ to Ca_2GeO_4 as

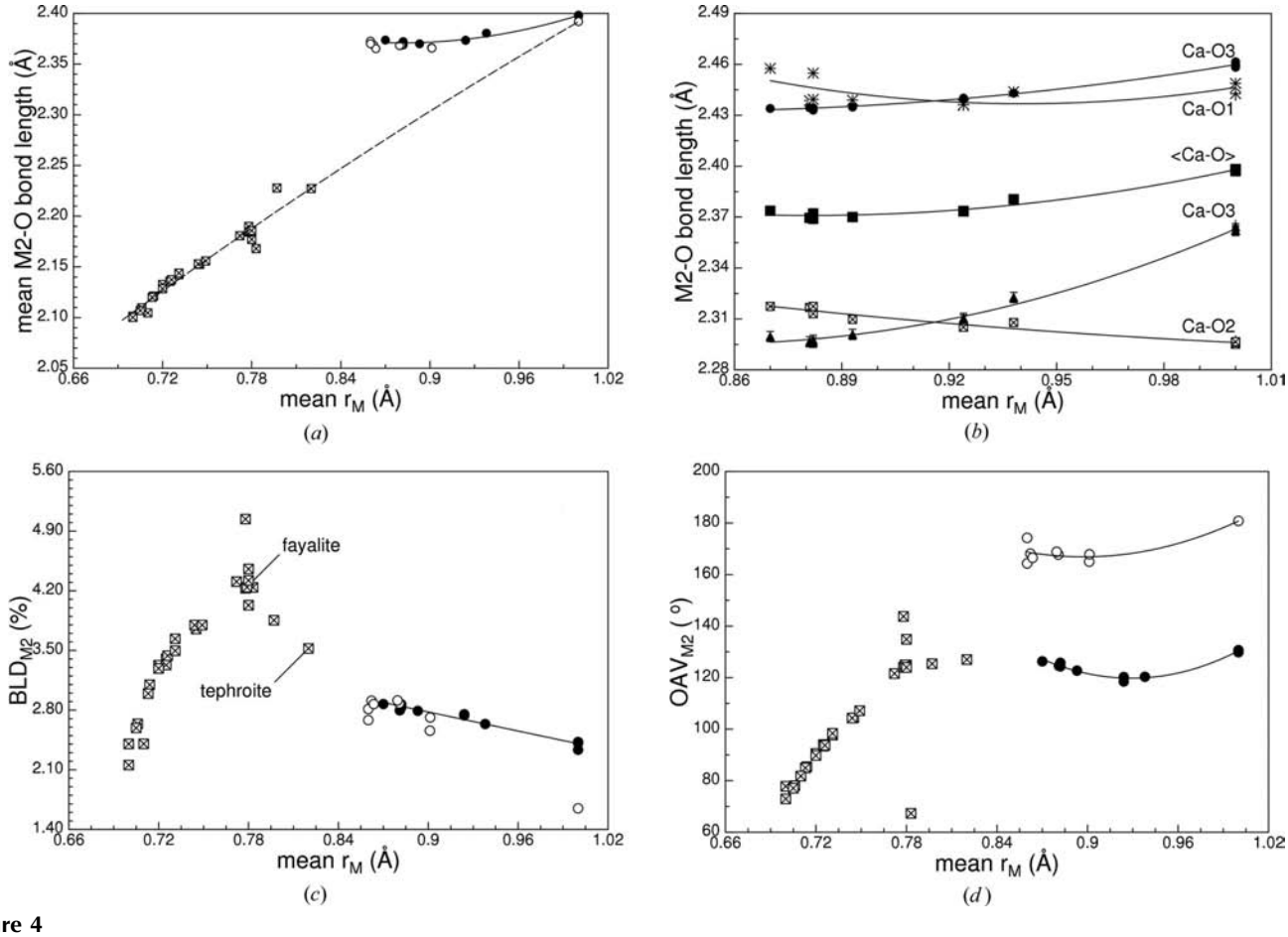

Figure 4
Variation of derived structural parameters with the average cationic radius of the *M*2 site for the Ge olivines of this study, partly in comparison with literature data: (*a*) average *M*2—O bond length, (*b*) individual *M*2—O bond lengths, (*c*) bond-length distortion (Renner & Lehmann, 1986) and (*d*) octahedral angle variance (Robinson *et al.*, 1971); symbols as in Fig. 2.

a direct consequence of *M*1-site cationic substitution; a similar large increase by 7.0% is found for the $O1^{v}\cdots O3^{i}$ edge, also strongly influenced by the *M*1 substitutions. Conversely, the $O3\cdots O3^{i}$ edge, common to the *M*2 and the tetrahedral sites, remains almost unaffected by the *M*1-site substitution; the $O3^{i}\cdots O3^{iii}$ edge, cross-linking two different *M*1 chains along the ⟨102⟩ direction, becomes shortened by 2.4%. The polyhedral distortion parameters OAV and OQE for the Ca germanate samples are both large but remain within the range 120–130° for OAV (Fig. 4*d*) and 1.034–1.037 for OQE, both parameters displaying a nonlinear (quadratic) variation. A similar dependency of OAV and OQE is valid for the Ca silicate olivines; however, here the *M*2 octahedron appears to be more distorted (Fig. 4*d*). It follows that the introduction of

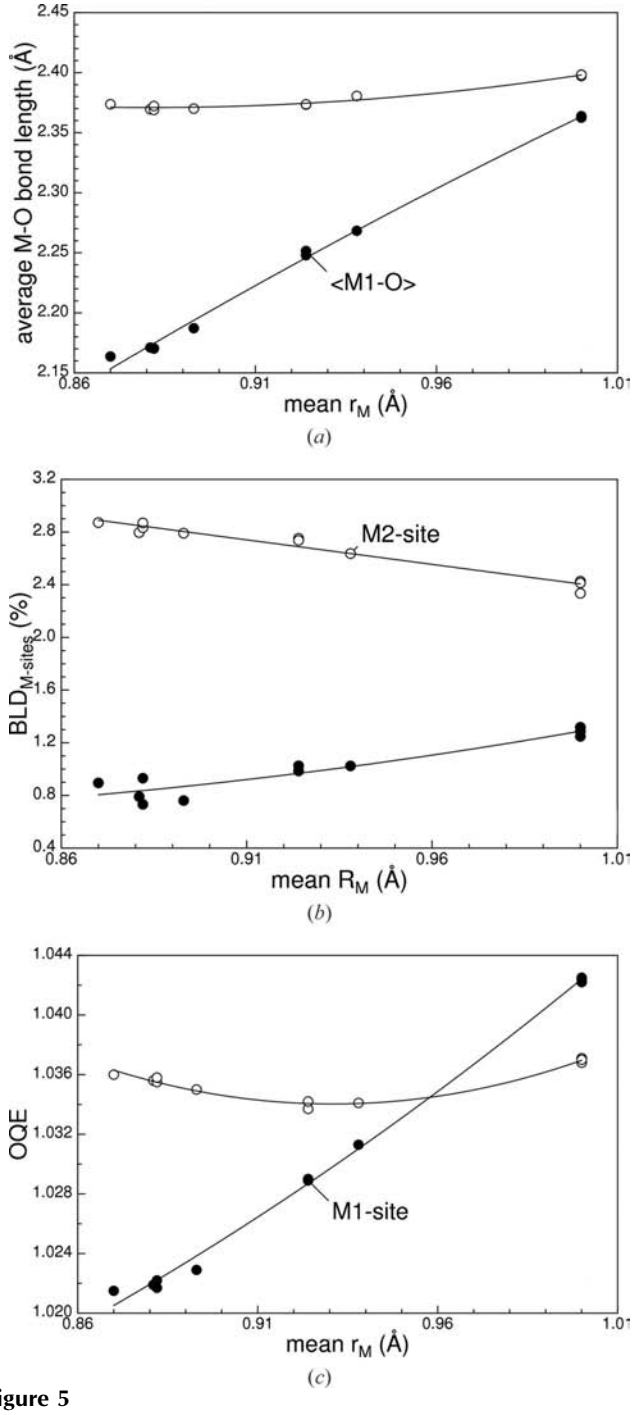

Figure 5
Comparison of the derived variation of structural parameters with the average cationic radius of the *M*1 and *M*2 sites for the Ge olivines of this study: (*a*) average *M*—O bond length, (*b*) bond-length distortion (Renner & Lehmann, 1986) and (*c*) octahedral quadratic elongation (Robinson *et al.*, 1971); symbols as in Fig. 2.

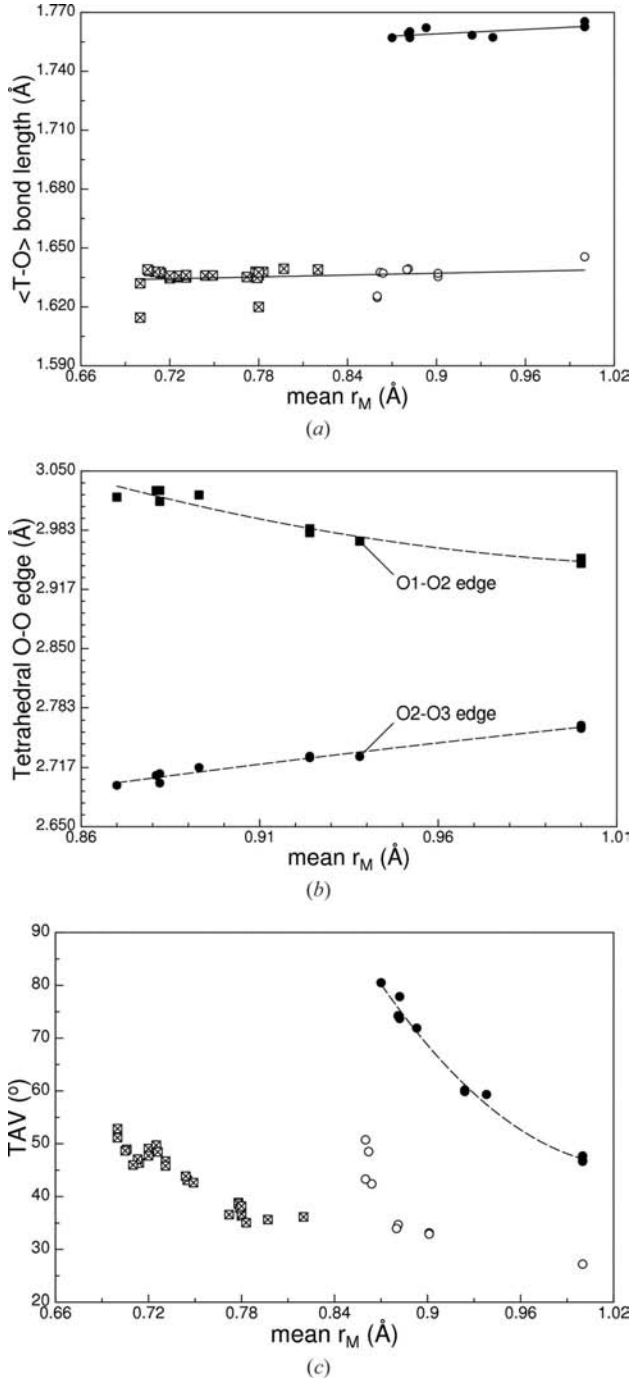

Figure 6
Variation of derived structural parameters with the average cationic radius of the tetrahedral site for the Ge olivines of this study, partly in comparison with literature data: (*a*) average *T*—O bond length, (*b*) individual tetrahedral O···O edges and (*c*) tetrahedral angle variance (Robinson *et al.*, 1971); symbols as in Fig. 2.

larger cations onto the *M*2 site increases the octahedral distortion on *M*2; the extrapolation of the data for the M_2SiO_4 olivine samples fits well the data for the Ca silicate olivines (Fig. 4*d*).

In conclusion, the variations in structural parameters on the *M*2 site are largely dominated by the variations on *M*1 and the tetrahedral site, and *M*2 acts as a buffer to keep the structural units of the *M*1 chain and the isolated tetrahedra fitting together.

It is generally accepted that the *M*2 polyhedron in olivine is the larger and more distorted polyhedron. This also holds true for most of the samples of this study, as indicated by the comparison of the variation of the average *M*1—O and *M*2—O bond lengths (Fig. 5*a*), the BLDs (Fig. 5*b*) and the OAVs (Fig. 5*c*). However, with increasing average cationic radius, *i.e.* towards the Ca_2GeO_4 composition, data for *M*1 and *M*2 approach each other, and in Ca_2GeO_4 the *M*2 polyhedron appears to be more regular than the *M*1 octahedron.

3.4. The tetrahedral site

Similarly to the *M*2 site, no substitution takes place on the tetrahedral site within the complete series; however, for the samples of this study, *T* is occupied by the distinctly larger Ge^{4+} [$r(Ge^{4+})$ = 0.40 Å], while it is occupied by Si^{4+} [$r(Si^{4+})$ = 0.26 Å; Shannon & Prewitt, 1969] in the two other series. This size difference of cations is, of course, reflected in the average *T*—O bond lengths, which, on the other hand, remain almost constant within the Ge^{4+} and the Si^{4+} series themselves (Fig. 6*a*). The differences in average *T*···O bonds between the silicate and the germanate olivines amount to ~0.13 to +0.15 Å and correlate with the differences in the ionic radii of the two cations. Individual *T*—O bond lengths do not show any significant variation with r_M and, regardless of the dimensional differences, silicate and germanate olivines possess very similar BLD parameters of around 0.5%. Distinct alterations with r_M are found for the O···O edges of the tetrahedron and – coupled with this – in the O—*T*—O bond angles. The O2···O3 edge, common to the tetrahedron and the *M*1 site, increases by 2.6% owing to the increase of the *M*1-octahedral size (Fig. 6*b*). Although this is the smallest variation with r_M for an *M*1-octahedral O···O edge, it is among the largest variations for the tetrahedral O···O edges. The O2—*T*—O3 angle, opposite to the aforementioned edge, increases by ~3% and approaches the ideal tetrahedral O—*T*—O bond angle. A second distinct variation with r_M is found for the unshared O1···O2 edge, which – in contrast to the O2···O3 edge – decreases by 2.5% from $CaMgGeO_4$ to Ca_2GeO_4; the angle opposite to this edge decreases but also becomes closer to the ideal tetrahedral bonding angle of 109.47°. As the O1···O2 edge links two different *M*1 chains along the **c** direction, the decrease of this edge can also be explained by the increasing size of the *M*1 cations (with increasing *M*1—O bond lengths), which exert dimensional strain onto this edge, thus shortening it. Similar variations of the O1···O2 and O2···O3 edges are also found for the silicate olivines; however, the trends are not as clearly defined as for the data of this study. The alterations in O—*T*—O angles directly affect the tetrahedral angle variance (TAV) and the tetrahedral quadratic elongation (TQE; Table 3), which both decrease distinctly with increasing r_M (Fig. 6*c*). While an increase of r_M causes the octahedra to become more distorted, the tetrahedra become more regular. This is also valid for the silicate olivine samples (Fig. 6*c*).

GJR gratefully acknowledges financial support by the 'Fonds zur Förderung der wissenschaftlichen Forschung (FWF)', Vienna, Austria, under grant R33-N10 (Erwin-Schrödinger Rückkehr-Stipendium).

References

Artioli, G., Rinalid, R., Wilson, C. C. & Zanazzi, P. F. (1995). *Am. Mineral.* **80**, 197–200.
Barbier, J. & Levy, D. (1997). *Z. Kristallogr.* **212**, 519–528.
Boström, D. (1987). *Am. Mineral.* **72**, 965–972.
Brown, G. E. Jr (1980). *Min. Soc. Am. Rev. Mineral.* **5**, 275–381.
Bruker (2001). *SMART-Plus* (Version 5.6) and *SAINT-Plus* (Version 5.0). Bruker AXS Inc., Madison, Wisconsin, USA.
Bykov, A. B., Petricevic, V., Steiner, J., Yao, Di., Isaacs, L. L., Kokta, M. R. & Alfano, R. R. (2000). *J. Cryst. Growth*, **211**, 295–301.
Deer, W. A., Howie, R. A. & Zussman, J. (1997). *Orthosilicates, Rock-Forming Minerals*, Vol. 1, 2nd ed. London: Geological Society Publishing House.
Della Giusta, A., Ottonello, G. & Secco, L. (1990). *Acta Cryst.* B**46**, 160–165.
Downs, R. T. (2005). *Commission on Powder Diffraction, International Union of Crystallography Newsletter*, **30**, 32–33.
Duijn, J. van, de Graaff, R. A. G. & Ijdo, D. J. W. (1995). *Mater. Res. Bull.* **30**, 1489–1493.
Eulenberger, G., Wittmann, A. & Nowotny, H. (1962). *Monatsh. Chem.* **93**, 1046–1054.
Farrugia, L. J. (1999). *J. Appl. Cryst.* **32**, 837–838.
Folco, L. & Mellini, M. (1997). *Eur. J. Mineral.* **9**, 964–973.
Francis, C. A. & Ribbe, P. H. (1980). *Am. Mineral.* **65**, 1263–1269.
Fujino, K., Sasaki, S., Takéuchi, Y. & Sadanaga, R. (1981). *Acta Cryst.* B**37**, 513–518.
Ghose, S. & Wan, C. (1974). *Contrib. Mineral. Petrol.* **47**, 131–140.
Hayward, C. L., Angel, R. J. & Ross, N. L. (1994). *Eur. J. Mineral.* **6**, 313–321.
Henderson, C. M. B., Knight, K. S., Redfern, S. A. T. & Wood, B. J. (1996). *Science*, **271**, 1713–1715.
ICSD (2006). Inorganic Crystal Structure Database. Fiz-Karlsruhe, Germany, and the National Institute of Standards and Technology (NIST), USA.
Kimata, M. & Nishida, N. (1987). *Neues Jahrb. Mineral. Monatsh.* pp. 160–170.
Lager, G. A. & Meagher, E. P. (1978). *Am. Mineral.* **63**, 365–377.
Losey, A., Rakovan, J., Hughes, J. M., Francis, J. M. & Dyar, M. D. (2004). *Can. Mineral.* **42,** 1105–1115.
Onken, H. (1965). *Tschermaks Mineral. Petrogr. Mitt.* **10**, 34–44.
Pennington, W. T. (1999). *J. Appl. Cryst.* **32**, 1028–1029.
Petit, P. E., Guyot, F., Fiquet, G. & Itié, J. P. (1996). *Phys. Chem. Miner.* **23**, 173–185.
Pilati, T., Demartin, F. & Gramaccioli, C. M. (1995). *Acta Cryst.* B**51**, 721–733.
Princivalle, F. & Secco, L. (1985). *Tschermaks Mineral. Petrogr. Mitt.* **34**, 105–115.
Redfern, S. A. T., Artioli, G., Rinaldi, R., Henderson, C. M. B., Knight, K. S. & Wood, B. J. (2000). *Phys. Chem. Miner.* **27**, 630–637.
Redfern, S. A. T., Henderson, M. B., Knight, K. S. & Wood, B. J. (1997). *Eur. J. Mineral.* **9**, 287–300.

Redhammer, G. J. & Roth, G. (2003). *Acta Cryst.* C**59**, i38–i40.
Redhammer, G. J. & Roth, G. (2006). *Acta Cryst.* C**62**, i61–i63.
Renner, B. & Lehmann, G. (1986). *Z. Kristallogr.* **175**, 43–59.
Reynard, B., Remy, C. & Takir, F. (1997). *Phys. Chem. Miner.* **24**, 77–84.
Rinaldi, R., Artioli, G., Wilson, C. C. & McIntyre, G. (2000). *Phys. Chem. Miner.* **27**, 623–629.
Rinaldi, R., Gatta, G. D., Artioli, G., Knight, K. S. & Geiger, C. A. (2005). *Phys. Chem. Miner.* **32**, 655–664.
Robinson, K., Gibbs, G. V. & Ribbe, P. H. (1971). *Science*, **172**, 567–570.
Shannon, R. D. & Prewitt, C. T. (1969). *Acta Cryst.* B**25**, 925–946.
Sharp, Z. D., Hazen, R. M. & Finger, L. W. (1987). *Am. Mineral.* **72**, 748–755.
Sheldrick, G. M. (2008). *Acta Cryst.* A**64**, 112–122.
Stoe & Cie (1996). *X-SHAPE* and *X-RED*. Stoe & Cie, Darmstadt, Germany.
Streltsov, V. A., Belokoneva, E. L., Tsirelson, V. G. & Hansen, N. K. (1993). *Acta Cryst.* B**49**, 147–153.
Weber, S. U., Grodzicki, M., Redhammer, G. J., Tippelt, G., Lottermoser, W. & Amthauer, G. (2007). *Phys. Chem. Miner.* **34**, 507–515.